HAL
open science

Oxidation behaviour of a CoNiCrAlY/h-BN based abradable coating

Justyna Elżbieta Jońca, Benoît Malard, Jérémy Soulié, Tom Sanviemvongsak, Serge Selezneff, Aurélie Vande Put

To cite this version:

Justyna Elżbieta Jońca, Benoît Malard, Jérémy Soulié, Tom Sanviemvongsak, Serge Selezneff, et al.. Oxidation behaviour of a CoNiCrAlY/h-BN based abradable coating. Corrosion Science, 2019, 153, pp.170-177. 10.1016/j.corsci.2019.02.030 . hal-02143137

HAL Id: hal-02143137

https://hal.science/hal-02143137v1

Submitted on 29 May 2019

HAL is a multi-disciplinary open access archive for the deposit and dissemination of scientific research documents, whether they are published or not. The documents may come from teaching and research institutions in France or abroad, or from public or private research centers.

L'archive ouverte pluridisciplinaire **HAL**, est destinée au dépôt et à la diffusion de documents scientifiques de niveau recherche, publiés ou non, émanant des établissements d'enseignement et de recherche français ou étrangers, des laboratoires publics ou privés.

Open Archive Toulouse Archive Ouverte (OATAO)

OATAO is an open access repository that collects the work of Toulouse researchers and makes it freely available over the web where possible

This is an author's version published in: http://oatao.univ-toulouse.fr/23914

Official URL: https://doi.org/10.1016/j.corsci.2019.02.030

To cite this version:

Jońca, Justyna Elżbieta and Malard, Benoît and Soulié, Jérémy and Sanviemvongsak, Tom and Selezneff, Serge and Vande Put, Aurélie *Oxidation behaviour of a CoNiCrAlY/h-BN based abradable coating.* (2019) Corrosion Science, 153. 170-177. ISSN 0010-938X

Any correspondence concerning this service should be sent to the repository administrator: tech-oatao@listes-diff.inp-toulouse.fr

Oxidation behaviour of a CoNiCrAlY/h-BN based abradable coating

Justyna Jońca[a], Benoît Malard[a], Jeremy Soulié[a], Tom Sanviemvongsak[a], Serge Selezneff[b], Aurelie Vande Put[a,*]

[a] CIRIMAT, Université de Toulouse, CNRS, INP- ENSIACET 4 allée Emile Monso - BP44362, 31030 Toulouse cedex 4, France
[b] Safran Aircraft Engines, Site de Corbeil, route Henri Auguste Desbruères, BP81, 91003 EVRY cedex, France

ARTICLE INFO

Keywords:
CoNiCrAlY/h-BN coating
Abradable coatings
Thermally grown oxides
High temperature oxidation resistance

ABSTRACT

The oxidation resistance of a thermally sprayed CoNiCrAlY/h-BN abradable coating was studied at 750 and 900 °C. First, the high porosity of the abradable coating was carefully characterised in order to estimate the specific surface area of the coating, required to evaluate the oxidation kinetics. Then the formed oxides were investigated by XRD, Raman spectroscopy and SEM. At 900 °C, the mass variations exhibited a deviation from parabolic behaviour due to rapidly growing oxides. Meanwhile, at 750 °C, after a transient state, the oxidation rate reaches a steady state, indicating that a protective alumina scale was maintained at this temperature.

1. Introduction

Abradable coatings are designed to preferentially wear out when in contact with a moving surface. For aircraft turbines, thermally sprayed coatings are preferred and used for gas path clearance control [1]. The clearance at the gas seal locations has a significant influence on the engine efficiency and therefore on the fuel consumption. Ideally, gas turbine engines would be produced with minimal clearance in the gas seal locations. However, these clearances are much larger to allow operation without catastrophic interaction between the rotor and the casing. Abradable coatings minimize these clearances without the risk of catastrophic failure.

Among many MCrAlY (where M = Ni and/or Co) abradable coatings, CoNiCrAlY showed improved oxidation and corrosion resistance up to 750 °C [2]. The microstructure of this coating exhibits three main phases, γ, γ' and β. The γ phase is a solid solution of Co, Ni, Cr and Al with a face centered cubic (FCC) structure [3]. The γ' Ni_3Al is a coherently precipitating phase with a face centered cubic (FCC) structure [4]. β is an intermetallic (Co,Ni)Al phase with a body centered cubic (BCC) structure [5]. Since the CoNiCrAlY matrix is harder than any of the rubbing blade materials, its abradability is ensured by the presence of macroporosity [2,6]. Porosity, in turn, is controlled through the amount of polyester that is thermally sprayed as a part of the coating and later removed by heat treatment after deposition. The abradability can be further improved by addition of solid lubricant, such as hexagonal boron nitride (h BN) [2], which has been found to be very stable at high temperatures up to 1000 °C [7].

Although few publications about oxidation behaviour of CoNiCrAlY abradable coatings have been published [6,8,9], a lot of researchers are investigating these as bond coatings for thermal barrier coating (TBC) systems. The specific composition of these coatings favours the formation of a thermally stable, adherent, continuous and slow growing layer of α Al_2O_3 at high temperatures [10 13]. However, the oxide scales on CoNiCrAlY coatings are not pure alumina and can also contain Y rich oxides and other oxides such as Cr_2O_3, NiO, CoO or $(Ni,Co)(Cr,Al)_2O_4$ spinel oxides [10]. The oxidation behaviour depends on the microstructure of the MCrAlY coatings, the manufacturing process and the working conditions [1]. Abradable coatings exhibit much higher porosity as compared to the dense bond coatings of the TBC systems. Therefore, due to this high porosity the mass variation due to oxidation can be much higher in the case of abradable materials.

This study concerns the oxidation behaviour of a thermally sprayed CoNiCrAlY/h BN abradable coating, whose maximum operating temperature is 750 °C [2]. Tests at higher temperatures were necessary to evaluate its capability for other applications. Therefore, isothermal oxidation tests were performed at 750 and 900 °C for a duration up to 500 h. The external oxide scales and the cross sections of the oxidized samples were characterised with X ray diffraction (XRD), Raman spectroscopy, energy dispersive X ray spectroscopy (EDS) analyses and scanning electron microscope (SEM) observations.

2. Experimental procedures

2.1. Experimental materials and equipments

The 718 alloy was used as a substrate (*c.a.* 4 mm thick). It was

* Corresponding author.
E-mail address: Aurelie.Rouaix@ensiacet.fr (A. Vande Put).

https://doi.org/10.1016/j.corsci.2019.02.030

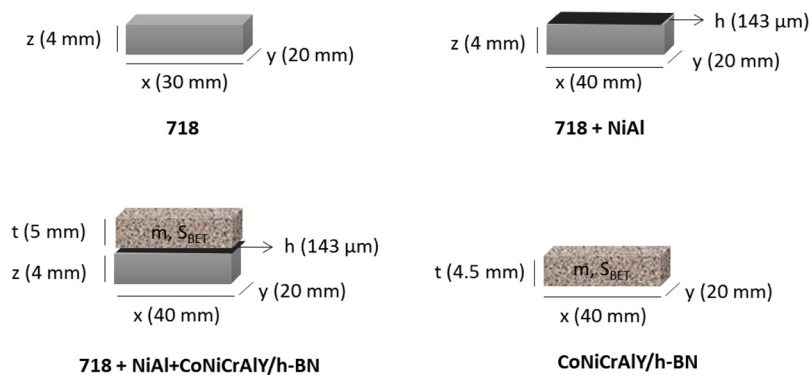

Fig. 1. Schematic representation of the samples prepared in this study.

ultrasonically cleaned in acetone and then grit blasted with alumina to enhance the adherence between the coating and the substrate. Nickel 5 wt.% Aluminum thermal spray powder (Metco 450NS, Oerlikon) was used as the feedstock powder for the fabrication of the NiAl coating. The NiAl sublayer accommodates the thermal expansion mismatch between the abradable coating and the substrate. It serves also as a rough undercoat helping attachment of the abradable coating. The CoNiCrAlY/h BN/polyester powder (Metco 2043, Oerlikon ; D90: 140 µm, D50: 75 µm, D10: 35 µm), with a composition of 30Co 25Ni 16Cr 6Al 0.3Y, 4 h BN, 15 polyester and 3 organic solids (in wt.%), was selected as the feedstock powder for the preparation of the CoNiCrAlY/h BN/polyester abradable coating. Both coatings were deposited by atmospheric plasma spraying (APS) on one side of the 718 substrate (Fig.1.). Finally, the whole system, *i.e.* 718 + NiAl + CoNiCrAlY/h BN/polyester was heat treated at 450 °C in order to burn away the polyester component and create porosity within the CoNiCrAlY/h BN coating and thus, to improve its abradability. The as prepared system was divided into smaller pieces of *c.a.* 20 mm x 40 mm by an electrical discharge machining procedure using CUT 20 P machine (GF AgieCharmilles) equipped with a Cu/Zn wire (Ø = 0.25 mm).

In addition to the complete system, *i.e.* 718 + NiAl + CoNiCrAlY/h BN, three other sets of samples were prepared, a 718 alloy without any coating, a NiAl coated 718 (718 + NiAl) and a CoNiCrAlY/h BN sample (Fig. 1). Those samples were prepared in order to perform necessary oxidation kinetics calculations and to complete characterizations. The 718 + NiAl sample was fabricated following the same procedure as described above, but without deposition of the CoNiCrAlY/h BN coating and thus, without the post deposition heat treatment. The CoNiCrAlY/h BN sample was prepared by removing the abradable layer from the 718 + NiAl + CoNiCrAlY/h BN system using a high performance tabletop cut off machine (Secotom 50, Struers). The system was cut in two pieces *c.a.* 0.5 mm above the NiAl layer (to make sure that none of it remained on the CoNiCrAlY/h BN sample). The 718 plate was cut into smaller pieces of *c.a.* 20 mm x 30 mm using the same machine to produce samples.

All prepared samples were ground using a manual polishing machine (Miniatech 263, Presi) with SiC abrasive papers with grades going from P80 to P600. All sides of the samples were ground except for the NiAl or CoNiCrAlY/h BN coated surfaces. Afterwards, the samples were cleaned with acetone and finally rinsed with ethanol in an ultrasonic bath for 5 min.

2.2. Estimation of the NiAl and CoNiCrAlY/h BN surface areas

Since, the CoNiCrAlY/h BN coating is very porous, its porosity (Section 2.2.1) and specific surface area (Section 2.2.2) were determined first to calculate properly its surface area. For the NiAl coating, in turn, its roughness must be considered (Section 2.2.3) to correctly estimate its surface area. Having these data, the surface areas of all studied systems were calculated (Section 2.3.).

2.2.1. CoNiCrAlY/h BN abradable porosity measurements

Porosity and pore size distribution were measured by mercury intrusion porosimetry using the AutoPore IV analyzer (Micrometrics), which allows detection of pores in the 0.003 600 µm range. The measurements were performed up to 414 MPa. In order to fit the measurement cell, the CoNiCrAlY/h BN abradable coating was divided into smaller pieces of *c.a.* 5 × 5 × 5 mm^3.

The total percentage porosity (P_{tot}) was calculated by:

$$P_{tot} = 100 d_{app} V_{Hg} \quad (1)$$

where d_{app} is the apparent density of the scaffold and V_{Hg} is the total mercury intrusion volume per gram of analysed specimen. The pore size distribution was calculated using the differential mercury intrusion volume plotted *versus* the pore size.

2.2.2. Estimation of the CoNiCrAlY/h BN abradable surface area

The critical step for the oxidation kinetics calculations was the estimation of the abradable surface. The CoNiCrAlY/h BN coating exhibits high surface area, which had to be considered in order to estimate the real surface in interaction with the environment. Therefore, its specific surface area was measured using a physisorption analysis with the Quantachrome Autosorb 1MP equipment. In order to fit the measurement cell, the abradable coating was divided into small pieces of *c.a.* 3 × 3 × 1 mm^3. Krypton gas was preferred to nitrogen gas to refine the measurement for values lower than 5 m^2/g, like in the case of this study. The obtained specific surface area (S_{BET}) was calculated using the multipoint BET model. S_{BET} was multiplied by the mass of the coating in order to obtain its total surface area. The mass of the coating, in turn, was calculated using the Eq. 12 (Section 2.3).

2.2.3. Estimation of the NiAl coating surface area

In order to correctly estimate the surface area of the NiAl coating, its roughness has to be considered. Therefore, its surface topography was investigated using a variation focus microscope (S neox, Sensofar, MAG 10X, 1 µm vertical resolution) equipped with SensoMAP software. A 3D surface numerical model that estimates the surface area by considering its roughness was developed by Sanviemvongsak et al. [14]. This method was used to approach the real surface area from roughness measurements and to take it into account for the analysis of oxidation kinetics. The model is built on the assumption that the surface presents periodic peaks and valleys, and thus can be represented as a 3D sinusoidal surface. This is a rough assumption that makes the modelling an approximation method to estimate surface area ratios. Two roughness parameters from the ISO 4287 (1993) standard were used. The first corresponds to the mean height parameter *Rc*, which characterizes the amplitude average of a profile ($\vec{z}$), and corresponds to the average of all maximum peak to valley heights (Zt_i) of profile elements, Eq. 2.

$$Rc = \frac{1}{m}\sum_{i=1}^{m} Zt_i \quad (2)$$

The second corresponds to the mean width parameter *Rsm*, which is the spatial or periodic parameter $(\vec{x}, \vec{y})$ which corresponds to the average width (XS_i) of profile elements, Eq. 3.

$$Rsm = \frac{1}{m}\sum_{i=1}^{m} XS_i \tag{3}$$

By controlling the amplitude $(\vec{z})$ and the periodicity of the signal/profile following two directions $(\vec{x}, \vec{y})$, the developed area can be associated with a sinusoidal "egg box" like model. From this model, its surface ratio was numerically determined using Matlab® software.

2.3. Surface area calculations

The surface areas of the described above systems were calculated as follows:

$$S_{718} = 2xy + 2xz + 2yz \tag{4}$$

$$S_{718+NiAl} = S'_{718} + S''_{NiAl} \tag{5}$$

$$S_{718+NiAl+CoNiCrAlY/h-BN} = S'_{718} + S'_{NiAl} + S'_{CoNiCrAlY/h-BN} \tag{6}$$

$$S_{CoNiCrAlY/h-BN} = S_{BET}\, m_{CoNiCrAlY/h-BN} \tag{7}$$

With x, y and z the width, the length and the thickness of the 718 substrate respectively, S_{BET} the specific surface area of the abradable coating (estimated as described in Section 2.2.2.), $m_{CoNiCrAlY/h-BN}$ the mass of the abradable coating alone, S_i the surface of the following systems: 718, 718 + NiAl, 718 + NiAl + CoNiCrAlY/h BN and CoNiCrAlY/h BN, S'_i and S''_i the surface of 718, NiAl and CoNiCrAlY/h BN materials when composing the various systems as described by Eqs. 8 11:

$$S'_{718} = xy + 2xz + 2yz \tag{8}$$

$$S'_{NiAl} = 2xh + 2yh \tag{9}$$

$$S'_{CoNiCrAlY/h-BN} = S_{BET}\, m'_{CoNiCrAlY/h-BN} - xy \tag{10}$$

$$S''_{NiAl} = xy + 2xh + 2yh \tag{11}$$

With h the thickness of the NiAl coating (estimated from the SEM images, see Fig. S1, Supporting Information), σ the surface parameter taking into account the roughness of the NiAl coating (estimated as described in Section 2.2.3., equal to 1.21 in this study), S'_{NiAl} the NiAl surface in the complete system and S''_{NiAl} the NiAl surface in the 718 + NiAl system. The mass of the abradable coating in the 718 + NiAl + CoNiCrAlY/h BN system ($m'_{CoNiCrAlY/h\ BN}$), in turn, was calculated using the following equation:

$$m'_{CoNiCrAlY/h-BN} = m_{718+NiAl+CoNiCrAlY/h-BN} - \rho_{NiAl} V'_{NiAl} - \rho_{718} V'_{718} \tag{12}$$

Where: $m_{718+NiAl+CoNiCrAlY/h\ BN}$ the total mass of the 718 + NiAl + CoNiCrAlY/h BN system, ρ_{NiAl}, ρ_{718} the density of the NiAl and 718 alloys respectively, and V'_{NiAl} and V'_{718} the volume of NiAl and 718 within the complete system respectively ($V'_{NiAl} = xyh$ and $V'_{718} = xyz$).

2.4. Isothermal oxidation tests

The isothermal oxidation tests were carried out in a Carbolite CWF 1300 furnace under laboratory air for 500 h. The specimens were oxidized at 750 and 900 °C, and then cooled to room temperature after 50, 100, 240 and 500 h, for weighing. The sensitivity of the balance (Sartorius ME215 P) was ± 0.02 mg. The oxidation behaviour was evaluated by plotting the mass variation per unit surface area as a function of the exposure time. Moreover, the parabolic oxidation rate constants (k_p) were determined for time intervals between 50 and 500 h and plotted on an Arrhenius diagram together with some reference data. These calculations were performed for individual alloy or coatings (*i.e.* 718 alloy, NiAl and CoNiCrAlY/h BN coatings). To do the latter, the following equations were used:

$$k_{p_i} = \left(\frac{\Delta m_i}{S_i}\right)^2 \frac{1}{t} \tag{13}$$

With Δm_i the mass variation of the whole system (718 + NiAl or 718 + NiAl + CoNiCrAlY/h BN) or a material of the system (718 or NiAl or CoNiCrAlY/h BN), S_i the corresponding surface and t the oxidation time. In the case of NiAl and CoNiCrAlY/h BN coatings, the corresponding mass variation was estimated based on the kinetics of the other materials composing the system, using Eqs. 14 17 respectively and Eqs. 8 and 9 (for the 718 and NiAl surface determination):

$$\Delta m_{NiAl} = \Delta m_{718+NiAl} - \Delta m_{718} \tag{14}$$

$$\Delta m_{NiAl} = \Delta m_{718+NiAl} - S'_{718}\sqrt{k_{p_{718}} t} \tag{15}$$

And

$$\Delta m_{CoNiCrAlY/h-BN} = \Delta m_{718+NiAl+CoNiCrAlY/h-BN} - \Delta m_{718} - \Delta m_{NiAl} \tag{16}$$

$$\Delta m_{CoNiCrAlY/h-BN} = \Delta m_{718+NiAl+CoNiCrAlY/h-BN} - S'_{718}\sqrt{k_{p_{718}} t} - S'_{NiAl}\sqrt{k_{p_{NiAl}} t} \tag{17}$$

With $k_{p_{718}}$ and $k_{p_{NiAl}}$ calculated for the corresponding time interval.

2.5. SEM observations, EDS, XRD and Raman spectroscopy characterization

The coating phases and oxides were identified by XRD with a D8 Advance Series 2 (Bruker) using Cu K_α radiation (λ = 0.15406 nm). The range of the scattering angles (2θ) was varied between 20° to 100°. Samples were continuously scanned with a step size of 0.03° (2θ) with 3 s per each step. XRD diffractograms were complemented by Raman spectroscopy using a LabRAM HR 800 (Horiba) spectrometer equipped with a confocal microscope. The analysis was performed between 100 and 1800 cm^{-1} and between 3700 and 4800 cm^{1}, the latter interval made it possible to follow the fluorescence signal of the Cr^{3+} ions as an impurity in the alumina, using a 532 nm laser. Observations of the reference and oxidized specimens were performed using a LEO 435 VP or FEI Quanta450 SEM equipped with an IMIX (PGT) or Quantax (Bruker) EDS, respectively. Two SEM observation modes were used, backscattered electrons (BSE) and secondary electrons (SE).

3. Results and discussion

3.1. Characterization of as sprayed coatings

Fig. 2 shows the XRD patterns of the feedstock CoNiCrAlY/h BN/polyester powder and the as sprayed CoNiCrAlY/h BN abradable coating. The diffraction peaks of the powder were attributed to the γ, γ' (γ Co Ni Cr matrix and γ' Ni_3Al) and β NiAl phases. The β NiAl was not

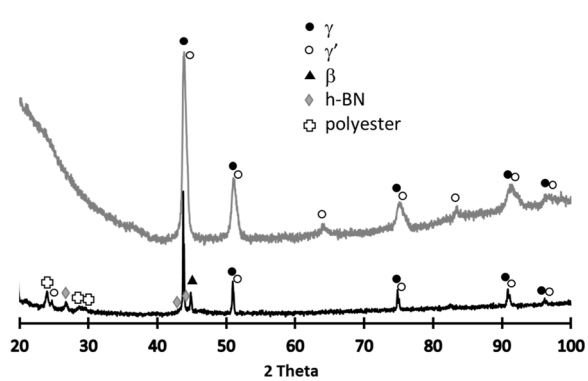

Fig. 2. XRD pattern of the CoNiCrAlY/h-BN/polyester feedstock powder (black) and the as-sprayed CoNiCrAlY/h-BN abradable coating (grey).

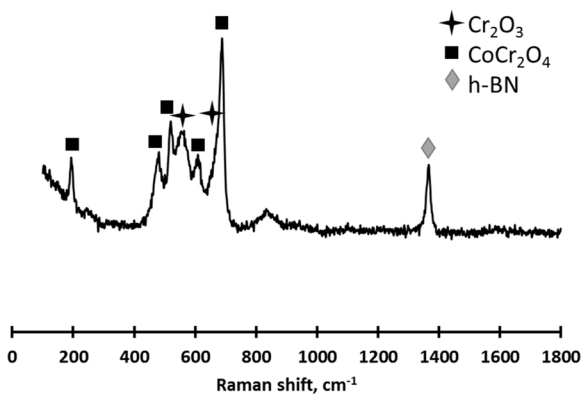

Fig. 3. Raman spectroscopy analyses of the as-sprayed CoNiCrAlY/h-BN abradable coating.

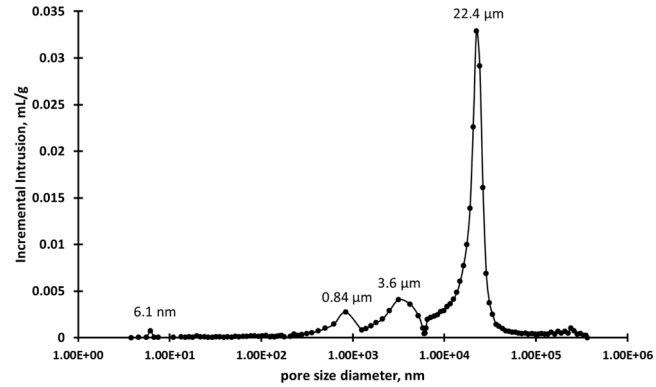

Fig. 5. Distribution of the pore diameter for the as-spayed CoNiCrAlY/h-BN abradable coating.

detected in the coating. Previous studies on CoNiCrAlY bond coatings pointed out that the β phase may dissolve into the γ matrix due to se vere plastic deformation of the particles upon impact with the substrate [15,16]. Some results indicate that the β NiAl phase did not have en ough time to precipitate within the γ matrix in the rapid solidification part of melted splats [17]. Some studies on CoNiCrAlY based thermal barrier coating systems showed that the β phase content increases upon increasing the content of unmelted particles. Since the β phase contains a large reservoir of Al, the presence of unmelted particles within the coating increases its oxidation resistance [18]. Note that some un melted particles were found within the whole thickness (*c.a.* 5 mm) of the CoNiCrAlY/h BN abradable coating prepared in this work (see below). However, their quantity and thus the proportion of the β NiAl phase was too small to be detected by XRD.

The XRD pattern of the feedstock powder exhibits peaks assigned to polyester. As expected, these peaks were not present in the XRD pattern of the CoNiCrAlY/h BN abradable coating due to the post spraying thermal treatment. The XRD pattern of the feedstock powder contains peaks that are attributed to the presence of h BN. These peaks are not observed in the diffractogram of the coating, but the h BN component was detected by Raman spectroscopy (Fig. 3).

Fig. 4 depicts the surface and cross sectional SEM observations of the as sprayed CoNiCrAlY/h BN abradable coating. It shows that this coating consisted of a lamellar structure, unmelted particles, pores and some oxides. It is a typical description of abradable coatings deposited by the thermal spray procedure [2]. The diameter of unmelted particles, estimated from SEM images, varied from 1.4 to 27.5 µm, whereas the diameter of the CoNiCrAlY particles from the feedstock CoNiCrAlY/h BN/polyester powder varied from 2.1 to 37.3 µm. The distribution of oxides was very heterogeneous and they were present across the entire thickness of the coating. EDS analysis shows that the dark grey areas correspond to Al and Y rich oxides. They can be easily distinguished from the mixed (Co,Ni,Cr,Al) rich oxides which exhibit a middle grey contrast. These oxides formed during the deposition process of the abradable coating. Their content seemed low as they were not present in the XRD diffractograms. However, Raman bands assigned to the $CoCr_2O_4$ spinel and Cr_2O_3 were observed (Fig. 3). The formation of similar oxides was also observed within an as sprayed CoNiCrAlY coating for thermal barrier coating systems [18].

The CoNiCrAlY/h BN coating exhibited a lamellar structure due to the deformation of melted particles upon contact with the substrate.

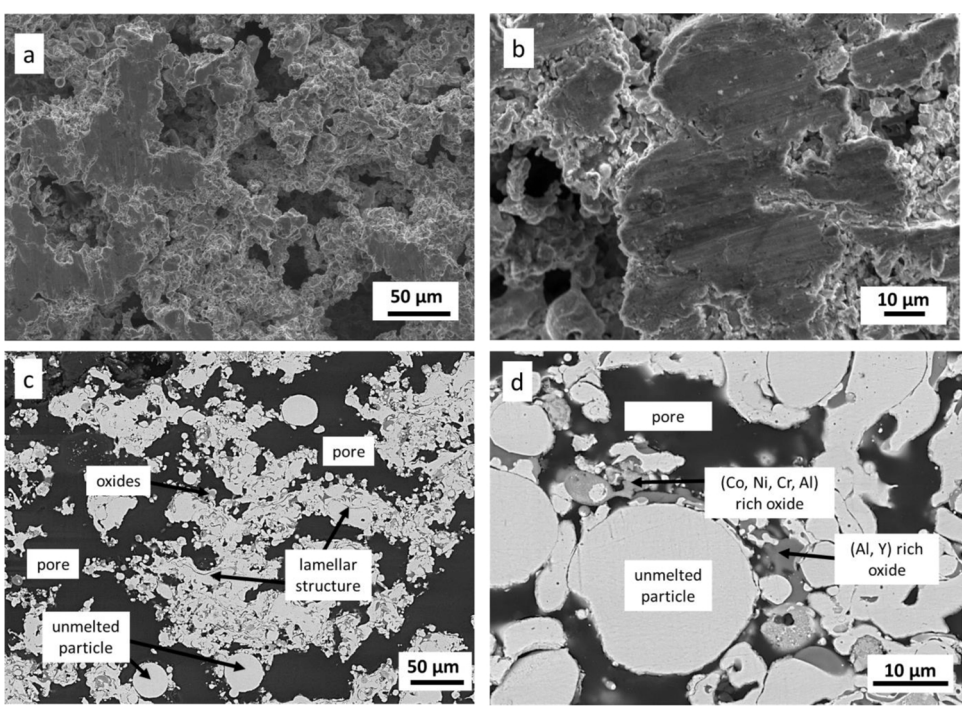

Fig. 4. Surface (a, b) and cross-sectional (c, d) SEM observations of the as-sprayed CoNiCrAlY/h-BN coating. (a) and (b) SE images, (c) and (d) BSE images.

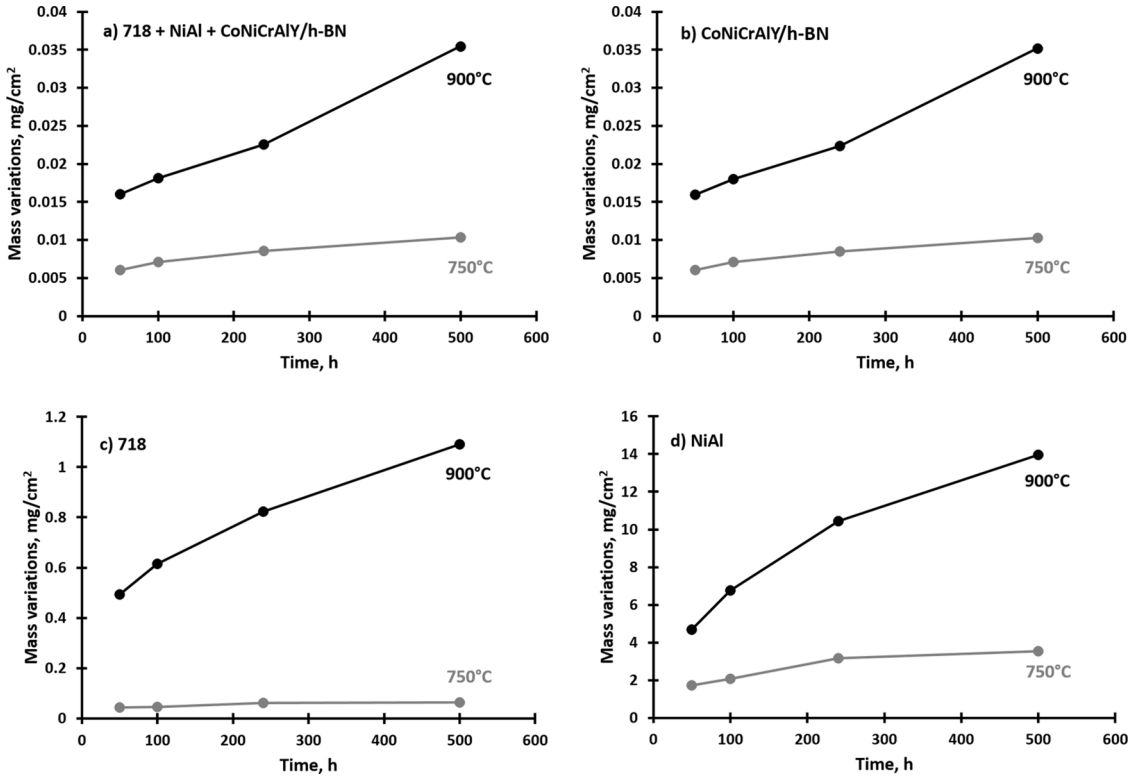

Fig. 6. Mass variations *versus* time for (a) the 718 + NiAl + CoNiCrAlY/h-BN sample, (b) the CoNiCrAlY/h-BN coating, (c) the 718 alloy and (d) the NiAl coating at 750 °C (grey symbols and line) and 900 °C (black symbols and line).

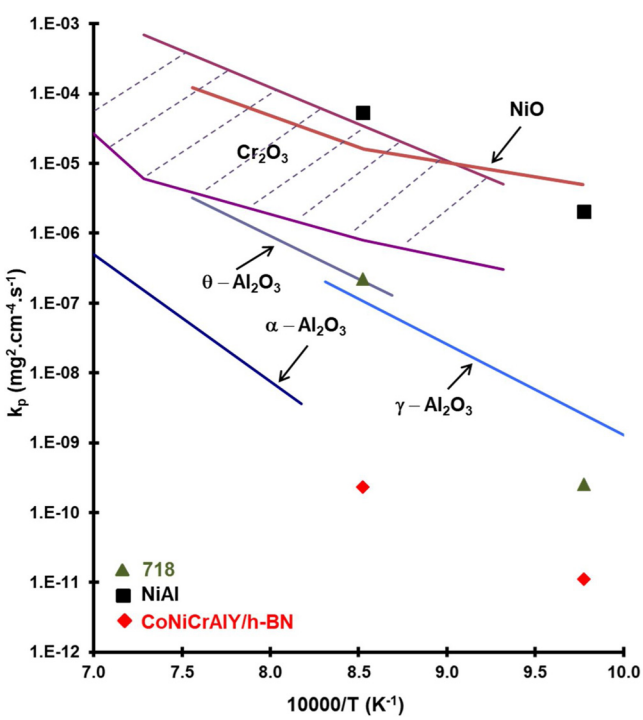

Fig. 7. Arrhenius diagram gathering k_p data obtained for the CoNiCrAlY/h-BN and NiAl coatings as well as for the 718 alloy, and literature data for Al_2O_3 [19], NiO [20] and Cr_2O_3 oxides [21]. The k_p values were determined for time interval between 50 h and 500 h.

The formation of pores and the quantity of porosity are controlled through the amount of entrapped polyester in the coating [2]. To create the desired porosity, the coating requires a polymer removal by post deposition heat treatment. As a result, a web like metallic structure is

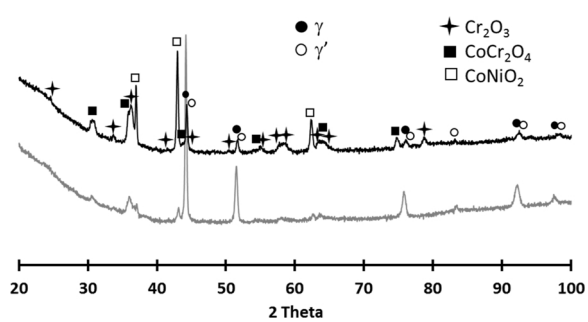

Fig. 8. XRD patterns of CoNiCrAlY/h-BN abradable coating after oxidation in air at 750 °C (grey) and 900 °C (black) for 500 h.

formed. This architecture allows excellent friability against titanium alloy, steel or superalloy blades. Coating porosity can vary from 35 to 60 vol.% [2]. In this study, the abradable coating exhibited a maximum porosity of 62 vol.% determined as explained above (Section 2.2.1). The distribution of the pore diameter is shown in Fig. 5. It is a tetramodal distribution with the pore diameters of 6.1 nm, 0.84 µm, 3.6 µm and 22.4 µm. The biggest pores mainly contribute to the total volume of porosity. This is consistent with the SEM pictures (Fig. 4. pores of several tens of microns) and characteristic of a macroporous material. The specific surface area of the abradable coating, equal to $0.6285\,m^2.\,g^{-1}$, is low for this kind of measurements but matches perfectly the pore size description above. The obtained value was multiplied by the coating mass in order to obtain the total surface area of the CoNiCrAlY/h BN abradable coating. Its mean value of $61{,}744.75\,cm^2$ is enormous compared to the bulk material and comes from the presence of macropores within the material.

Fig. S2. shows the XRD pattern of the as sprayed NiAl coating. The diffraction peaks can be attributed mainly to the γ phase. Fig. S1 depicts the surface and cross sectional SEM observations of this coating. The surface of the coating is quite rough and its roughness was accounted

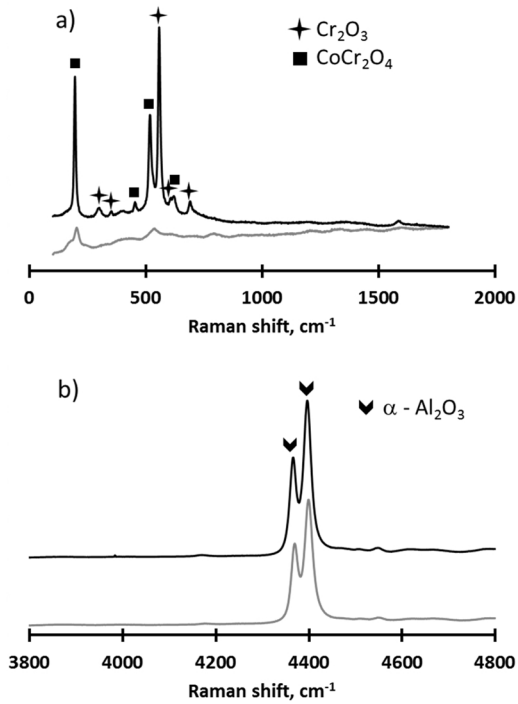

Fig. 9. (a) Raman spectroscopy and (b) fluorescence spectroscopy of the CoNiCrAlY/h-BN abradable coating after oxidation in air at 750 °C (grey) and 900 °C (black) for 500 h.

for in the surface area calculations (as explained in Section 2.2.3). Its mean surface area of 9.23 cm^2 was 1.2 times larger than the smooth material. The average thickness of the NiAl coating was 143 µm and consisted of lamellar structured, unmelted particles of a Ni rich matrix and Al rich oxides. These oxides formed during the coating deposition.

3.2. Oxidation kinetics

The mass variations of the 718 + NiAl + CoNiCrAlY/h BN sample oxidized under laboratory air at 750 and 900 °C are shown in Fig. 6a. At 900 °C, the sample exhibited three stages during the oxidation process. A transient growth stage occurred within the first hours, but since the first withdrawal of the sample was performed after 50 h, the corre sponding data points are not recorded. Afterwards, the oxidation rate briefly decreased, followed by a high mass gain rate between 240 and 500 h. As seen in Fig. 6b, the curves for the CoNiCrAlY/h BN coating exhibit a similar behaviour. A similar trend was also described for a thermal barrier coating system based on a CoNiCrAlY/h BN coating oxidized at 1100 °C [18]. Such behaviour was not observed for the samples oxidized at 750 °C, indicating that the coating withstood well this temperature (Fig. 6a, b).

The 718 alloy and NiAl coating exhibited higher growth rates as compared to the CoNiCrAlY/h BN coating as seen in Fig. 6b, 6c and 6d. The Arrhenius diagram (Fig. 7), from which the oxidation kinetics are determined using eq. 13, suggests that at 900 °C in air the 718 alloy forms chromia, whereas the NiAl coating forms NiO the oxide with the fastest oxide scale growth observed in this study. This was confirmed by XRD analysis (see Supporting Informations, Fig. S4). The CoNiCrAlY/h BN coating presented the lowest oxidation kinetics in this study with k_p values of 1.12×10^{-11} $mg^2.cm^{-4}.s^{-1}$ and 2.29×10^{-10} $mg^2.cm^{-4}.s^{-1}$ at 750 and 900 °C, respectively. The k_p values were determined for time interval between 50 and 500 h. To refine kinetics calculation, the evolution of the abradable coating surface area due to oxidation could be taken into account. However, in this study, all calculations were done with the initial surface areas (*i.e.* before oxidation).

3.3. Characterization of coatings after oxidation

Fig. 8 shows the XRD patterns of the CoNiCrAlY/h BN abradable coatings after oxidation at 750 and 900 °C for 500 h. The γ and γ' phases, Cr_2O_3, $CoNiO_2$ and $CoCr_2O_4$ oxides were found on the coating surface after oxidation. The quantity of oxides increased with in creasing temperature. Indeed, the corresponding XRD peak intensities were much higher at 900 °C than at 750 °C. The Raman spectroscopy

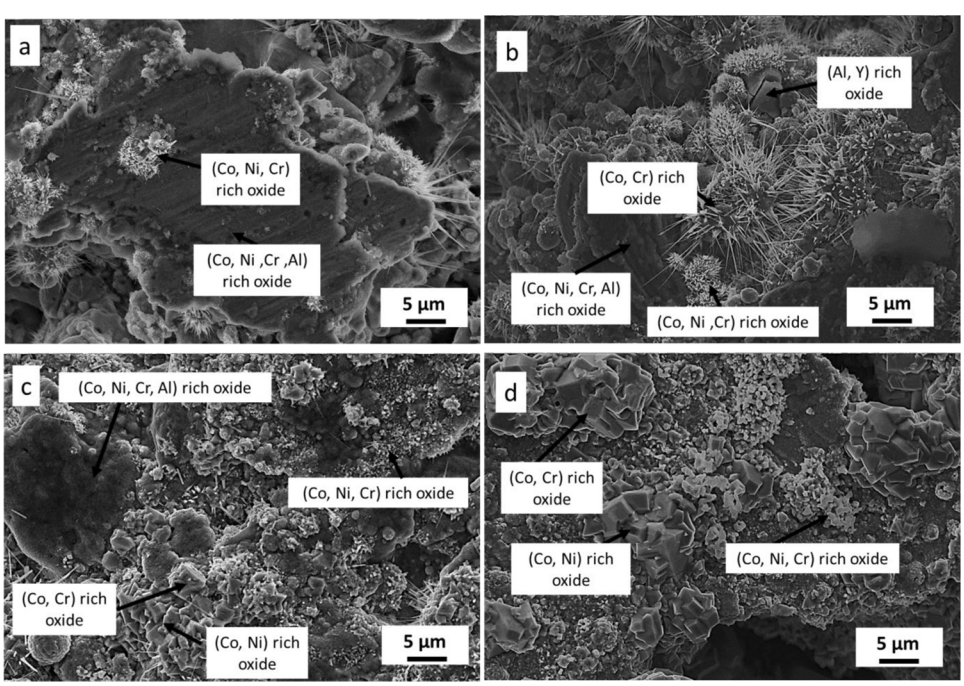

Fig. 10. SEM observations of the surface of CoNiCrAlY/h-BN abradable coatings after oxidation at 750 °C (a, b) and 900 °C (c, d) for 100 h (a, c) and 500 h (b, d). Observations realized using the SE detector.

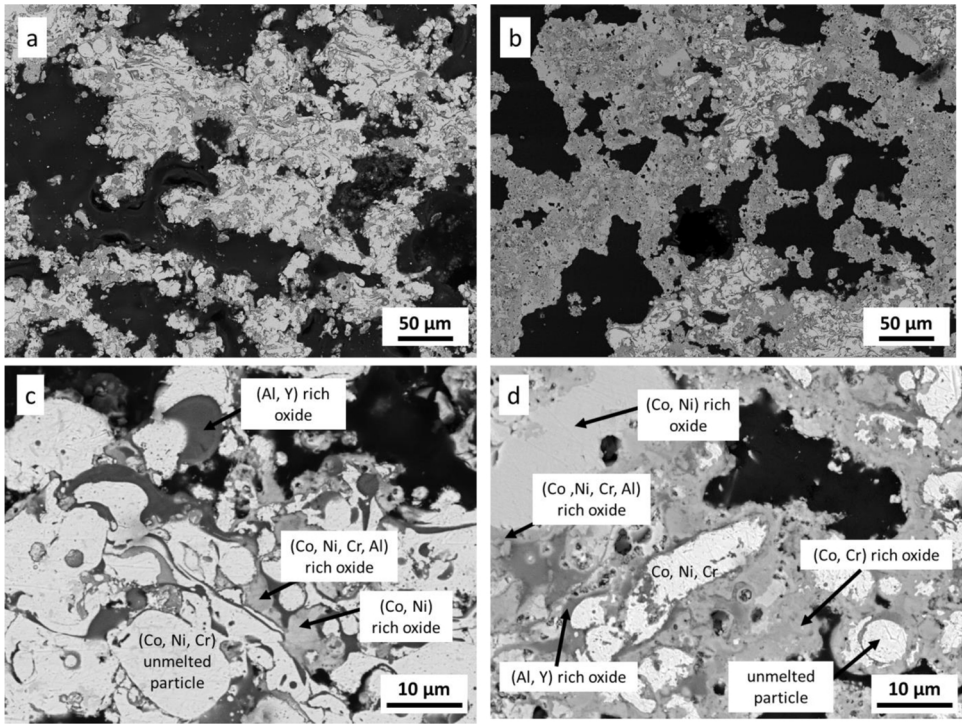

Fig. 11. Cross-sectional SEM observations of CoNiCrAlY/h-BN abradable coatings after oxidation in air at 750 °C (a, c) and 900 °C (b, d) for 500 h. Observations realized using the BSE detector.

results confirmed the presence of Cr_2O_3 and $CoCr_2O_4$ (Fig. 9a) while the fluorescence spectroscopy analysis revealed the presence of α Al_2O_3 within the abradable coating (Fig.9b). A continuous scale of Al_2O_3 acts as a diffusion barrier to protect the coating from further oxidation, thereby increasing the service life of the coating at elevated temperatures [22 25]. However, due to alumina scale formation, the Al content within the coating decreases with time. Below a critical level of Al within the coating, rapidly growing oxides such as NiO, Cr_2O_3 and $(Ni,Co)(Al,Cr)_2O_4$ start to nucleate [26,27], which can cause deviation from a classical parabolic behaviour of the mass variations, as noted in this study (Fig.6a, b) and during previous investigations [18].

Fig. 10 presents surface morphology of the abradable coating after oxidation at 750 and 900 °C for 100 and 500 h. The oxide grain size increased considerably with temperature and oxides exhibited polyhedral structures at 900 °C, mainly (Co,Ni) or (Co,Cr) rich oxides. At 750 °C, another interesting morphology can be observed, *i.e.* long needles. Some of them were also present after oxidation at 900 °C for 100 h, but none were observed after 500 h at this temperature. The presence of well defined needles at 750 °C can be assigned to the formation of metastable θ Al_2O_3 during initial steps of oxidation that transforms irreversibly into α Al_2O_3 with time without changing its morphology [19]. At 900 °C, the content of the needles decreased due to the accelerated transformation from θ Al_2O_3 to α Al_2O_3 at this temperature [28].

Fig. 11 presents the cross sectional images of the CoNiCrAlY/h BN abradable coatings after oxidation at 750 and 900 °C for 500 h. As shown by EDS analysis, the (Al,Y) rich oxides exhibit a dark grey contrast while the (Co,Ni) , (Co,Cr) and (Co,Ni,Cr,Al) rich oxides exhibit a medium grey contrast. As expected, the content of the oxides, especially the rapidly growing oxides, increased with increasing temperature. The oxides were present in the whole volume of the coating. One can note that the (Al,Y) rich oxides appear mainly around unmelted particles and lamellar structures. The interior of these structures remains metallic, but with a reduced quantity of Al. The latter diffused to the surface of the particles and lamellar structures and created a protective Al_2O_3 layer [18]. It suggests that the unmelted particles exhibit a larger Al reservoir than the surrounding material. This explains the differences in the oxidation behaviour between different parts of the abradable coating and the heterogeneous oxide distribution. However, as explain previously, unmelted particles represent only a very small proportion of the coating. Such heterogeneous behaviour is therefore locally observed.

4. Conclusions

The high temperature oxidation resistance of a thermally sprayed CoNiCrAlY/h BN abradable coating was studied at 750 and 900 °C. The as sprayed coating exhibited a lamellar structure, unmelted particles, pores and some oxides (mainly (Al,Y) rich oxides and (Co,Ni,Cr,Al) rich oxides). The enormous surface area of the coating resulting from its high porosity was carefully characterised and then taken into account in the kinetics calculations. After 500 h at 900 °C in laboratory air, the mass variations exhibited deviation from a classical parabolic behaviour, indicating oxide growth acceleration mainly due to the formation of rapidly growing oxide. These oxides were distributed across the whole volume of the coating, except for some unmelted particles observed locally across the coating thickness. The latter exhibited a large reservoir of Al which allowed the formation of a protective, thin and adherent alumina scale around the particles making them resistant to oxidation.

Data availability

The raw/processed data required to reproduce these findings cannot be shared at this time due to the industrial character of our study.

Acknowledgments

We would like to thank Safran Aircraft Engines (Site de Corbeil, Evry, France) for the financial support. We thank Alain Castillo from the GET OMP laboratory and David Neumeyer from the CEMES laboratory in Toulouse for the BET specific surface analysis. We acknowledge

Gwenaelle Guittier from the SAP LGC laboratory in Toulouse for the macroporosity measurements. We thank our technicians and engineers Cedric Charvillat, Alexandre Freulon, Remi Garcia, Ronan Mainguy, Djar Oquab and Yannick Thebault for their precious help in setting up the experiments.

Appendix A. Supplementary data

Supplementary material related to this article can be found, in the online version, at doi:https://doi.org/10.1016/j.corsci.2019.02.030.

References

[1] W. Brandl, D. Toma, H.J. Grabke, The characteristics of alumina scales formed on HVOF-sprayed MCrAlY coatings, Surf. Coat. Technol. 108–109 (1998) 10–15, https://doi.org/10.1016/S0257-8972(98)00613-6.

[2] S. Wilson, Thermally sprayed abradable coating technology for sealing in gas turbines, The Future of Gas Turbine Technology, 6th International Conference (2012) Paper ID Number 51.

[3] P. Poza, P.S. Grant, Microstructure evolution of vacuum plasma sprayed CoNiCrAlY coatings after heat treatment and isothermal oxidation, Surf. Coat. Technol. 201 (2006) 2887–2896, https://doi.org/10.1016/j.surfcoat.2006.06.001.

[4] B.G. Mendis, B. Tryon, T.M. Pollock, K.J. Hemker, Microstructural observations of as-prepared and thermal cycled NiCoCrAlY bond coats, Surf. Coat. Technol. 201 (2006) 3918–3925, https://doi.org/10.1016/j.surfcoat.2006.07.249.

[5] M. Mohammadi, S. Javadpour, A. Kobayashi, S.A. Jenabali Jahromi, K. Shirvani, Thermal shock properties and microstructure investigation of LVPS and HVOF-CoNiCrAlYSi coatings on the IN738LC superalloy, Vacuum 88 (2013) 124–129, https://doi.org/10.1016/j.vacuum.2012.02.003.

[6] D. Sporer, S. Wilson, P. Fiala, R. Schuelein, Thermally sprayed abradable coatings in steam turbines : design integration and functionality testing, ASME Turbo Expo 2010: Power for Land, Sea, and Air Volume 7: Turbomachinery, Parts A, B, and C (2010) 2309–2317, https://doi.org/10.1115/GT2010-23568.

[7] N. Kostoglou, K. Polychronopoulou, C. Rebholz, Thermal and chemical stability of hexagonal boron nitride (h-BN) nanoplatelets, Vacuum 112 (2015) 42–45, https://doi.org/10.1016/j.vacuum.2014.11.009.

[8] U. Bardi, C. Giolli, A. Scrivani, G. Rizzi, F. Borgioli, A. Fossati, K. Partes, T. Seefeld, D. Sporer, A. Refke, Development and Investigation on New Composite and Ceramic Coatings as Possible Abradable Seals, J. Therm. Spray Technol. 17 (2008) 805–811, https://doi.org/10.1007/s11666-008-9246-5.

[9] D. Aussavy, R. Bolot, F. Peyraut, G. Montavon, S. Selezneff, Thermomechanical Properties of CoNiCrAlY-BN-Polyester Composite Coatings Elaborated by Atmospheric Plasma Spraying, Key Eng. Mater. 606 (2014) 167–170, https://doi.org/10.4028/www.scientific.net/KEM.606.167.

[10] T.J. Nijdam, C. Kwakernaak, W.G. Sloof, The effects of alloy microstructure refinement on the short-term thermal oxidation of NiCoCrAlY alloys, Metall. Mater. Trans. A 37 (2006) 683–693, https://doi.org/10.1007/s11661-006-0040-z.

[11] G. Marginean, D. Utu, Cyclic oxidation behaviour of different treated CoNiCrAlY coatings, Appl. Surf. Sci. 258 (2012) 8307–8311, https://doi.org/10.1016/j.apsusc.2012.05.050.

[12] S. Nath, I. Manna, J.D. Majumdar, Kinetics and mechanism of isothermal oxidation of compositionally graded yttria stabilized zirconia (YSZ) based thermal barrier coating, Corros. Sci. 88 (2014) 10–22, https://doi.org/10.1016/j.corsci.2014.06.050.

[13] S. Salam, P.Y. Hou, Y.-D. Zhang, H.-F. Wang, C. Zhang, Z.-G. Yang, Compositional effects on the high-temperature oxidation lifetime of MCrAlY type coating alloys, Corros. Sci. 95 (2015) 143–151, https://doi.org/10.1016/j.corsci.2015.03.011.

[14] T. Sanviemvongsak, D. Monceau, B. Macquaire, High temperature oxidation of IN 718 manufactured by Laser Beam Melting and Electron Beam Melting: effect of surface topography, Corros. Sci. 141 (2018) 127–145, https://doi.org/10.1016/j.corsci.2018.07.005.

[15] P. Richer, M. Yandouzi, L. Beauvais, B. Jodoin, Oxidation behaviour of CoNiCrAlY bond coats produced by plasma, HVOF and cold gas dynamic spraying, Surf. Coat. Technol. 204 (2010) 3962–3974, https://doi.org/10.1016/j.surfcoat.2010.03.043.

[16] P. Richer, A. Zúñiga, M. Yandouzi, B. Jodoin, CoNiCrAlY microstructural changes induced during Cold Gas Dynamic Spraying, Surf. Coat. Technol. 203 (2008) 364–371, https://doi.org/10.1016/j.surfcoat.2008.09.014.

[17] S. Saeidi, K. Voisey, D. Mccartney, The effect of heat treatment on the oxidation behavior of HVOF and VPS CoNiCrAlY coatings, J. Therm. Spray Technol. 18 (2009) 209–216, https://doi.org/10.1007/s11666-009-9311-8.

[18] J.J. Tang, Y. Bai, J.C. Zhang, K. Liu, X.Y. Liu, P. Zhang, Y. Wang, L. Zhang, G.Y. Liang, Y. Gao, J.F. Yang, Microstructural design and oxidation resistance of CoNiCrAlY alloy coatings in thermal barrier coating system, J. Alloys Compd. 688 (2016) 729–741, https://doi.org/10.1016/j.jallcom.2016.07.018.

[19] M.W. Brumm, H.J. Grabke, The oxidation behaviour of NiAl-I. Phase transformations in the alumina scale during oxidation of NiAl and NiAl-Cr alloys, Corros. Sci. 33 (1992) 1677–1690, https://doi.org/10.1016/0010-938X(92)90002-K.

[20] L. Berry, J. Paidassi, Contribution à l'étude de l'oxydation du nickel aux températures élevées, Sci. Rev. Metall. 65 (1968) 651.

[21] H. Hindam, D.P. Whittle, Microstructure, adhesion and growth kinetics of protective scales on metals and alloys, Oxid. Met. 18 (1982) 245–284, https://doi.org/10.1007/BF00656571.

[22] Y. Bai, C. Ding, H. Li, Z. Han, B. Ding, T. Wang, L. Yu, Isothermal oxidation behavior of supersonic atmospheric plasma-sprayed thermal barrier coating system, J. Therm. Spray Technol. 22 (2013) 1201–1209, https://doi.org/10.1007/s11666-013-9979-7.

[23] W.R. Chen, X. Wu, B.R. Marple, P.C. Patnaik, The growth and influence of thermally grown oxide in a thermal barrier coating, Surf. Coat. Technol. 201 (2006) 1074–1079, https://doi.org/10.1016/j.surfcoat.2006.01.023.

[24] W.R. Chen, X. Wu, B.R. Marple, R.S. Lima, P.C. Patnaik, Pre-oxidation and TGO growth behaviour of an air-plasma-sprayed thermal barrier coating, Surf. Coat. Technol. 202 (2008) 3787–3796, https://doi.org/10.1016/j.surfcoat.2008.01.021.

[25] W. Chen, X. Wu, P. Patnaik, B.R. Marple, D.R. Nagy, TGO growth behaviour in TBCs with APS and HVOF bond coats, Surf. Coat. Technol. 202 (2008), https://doi.org/10.1016/j.surfcoat.2007.09.042.

[26] M. Daroonparvar, M.A.M. Yajid, N.M. Yusof, M.S. Hussain, H.R.B.- Rad, Formation of a dense and continuous Al2O3 layer in nano thermal barrier coating systems for the suppression of spinel growth on the Al2O3 oxide scale during oxidation, J. Alloys Compd. 571 (2013) 205–220, https://doi.org/10.1016/j.jallcom.2013.03.168.

[27] Y.J. Han, F.X. Ye, G.X. Lu, C. Liu, L.J. Hao, Residual stress evolution of thermally grown oxide in thermal barrier coatings deposited onto nickel-base superalloy and iron-base alloy with thermal exposure ageing, J. Alloys Compd. 584 (2014) 19–27, https://doi.org/10.1016/j.jallcom.2013.08.144.

[28] S. Kitaoka, T. Kuroyama, M. Matsumoto, R. Kitazawa, Y. Kagawa, Control of polymorphism in Al2O3 scale formed by oxidation of alumina-forming alloys, Corros. Sci. 52 (2010) 429–434, https://doi.org/10.1016/j.corsci.2009.09.031.